Hindawi Publishing Corporation
International Journal of Photoenergy
Volume 2012, Article ID 104597, 8 pages
doi:10.1155/2012/104597

Research Article

Influence of Electrolyte Refreshing on the Photoelectrochemical Performance of Fiber-Shaped Dye-Sensitized Solar Cells

Zhibin Lv, Hongwei Wu, Xin Cai, Yongping Fu, Dan Wang, Zengze Chu, and Dechun Zou

Beijing National Laboratory for Molecular Sciences, Key Laboratory of Polymer Chemistry and Physics of Ministry of Education, College of Chemistry and Molecular Engineering, Peking University, Beijing 100871, China

Correspondence should be addressed to Dechun Zou, dczou@pku.edu.cn

Received 2 October 2011; Accepted 30 November 2011

Academic Editor: Gerrit Boschloo

Given the convenient sealing of fiber-shaped dye-sensitized solar cells (FDSSCs), the electrolyte refreshing effect on the photoelectrochemical performance of FDSSCs was studied. The electron transport and interfacial recombination kinetics were also systematically investigated by electrochemical impedance spectroscopy. With increased electrolyte refreshing times from 0 to 10, the open-circuit voltage (V_{oc}) and fill factor (FF) increased, whereas the photocurrent density (J_{sc}) and power conversion efficiency (PCE) significantly decreased. The increased V_{oc} was mainly ascribed to the electron recombination resistance ($R_{ct,\,WE}$) at the TiO_2/electrolyte interface and electron lifetime. The decreased J_{sc} and PCE were due to dye desorption and the increase of series resistance. Further investigation proved that Li^+ played a vital role in increasing V_{oc} as electrolyte refreshing and Li^+ had more significant impact than TBP (tert-butyl pyridine) on maintaining high V_{oc}.

1. Introduction

Given their high-energy conversion efficiency and simple fabrication process, dye-sensitized solar cells (DSSCs) have been attracting worldwide scientific and technological interest for decades [1–3]. Research on the optimization of materials and fabrication procedures is progressive.

Consequently, current planar DSSCs using I_3^-/I^- electrolytes, have achieved up to 11%-12% conversion efficiency [4–6], and the efficiency of large-scale modules has also reached 8% with aperture areas of more than 20 cm^2 [7]. DSSCs are considered as promising alternatives to conventional silicon-based photovoltaic devices for sustainable, low-cost, and environment-friendly energy supply. However, there are still obstacles to overcome, such as cost, limited efficiency in the large-scale module, electrolyte leakage, cell sealing, and stability.

Fiber solar cells have received great attention in recent years [8–22]. Their advantages over DSSCs having traditional sandwiched planar structure include the following. (1) Nonflat structured solar cells get rid of the dependence on transparent conductive oxides (TCOs) [8]. Traditional solar cells and the reported tubular solar cells still use TCOs, which usually account for 30%–50% of total cell costs [23]. (2) The fiber cell is a macro-one-dimensional structure, and has a smaller package area ratio than the two-dimensional structure. Making a larger cell only requires increasing the length of the cell. When the cell is increased to a certain size, the package area of the cell remains basically unchanged [20]. (3) The flexible fiber cell can directly adopt the traditional preparation technology. In contrast, special technologies must be adopted to create all kinds of traditional flexible flat cells (like OPVs and planar DSSCs) to ensure that the flexible substrate will not be damaged during the preparation process, such as low temperatures. (4) Existing textile techniques can be directly used in weaving for the mass production of fiber cells. This method is another further improvement of the traditional roll-to-roll technology for producing flexible electronic devices [18, 24].

The advancements in fiber solar cells, including fiber-shaped organic solar cells and fiber-shaped DSSCs (FDSSCs), have thus far been impressive [8, 9, 11]. The highest power

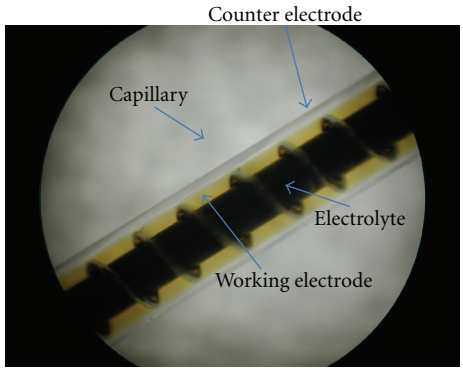

Figure 1: An optical photo of FDSSC structure details.

efficiency of FDSSCs ever reported is above 7% [18]. FDSSCs not only address the problems of traditional flat cells, but also provide some new features to elucidate the factors that affect their performances. For example, Fu et al. [18] have studied the three-dimensional light collecting ability of FDSSCs. FDSSCs are found to be able to harvest surrounding light efficiently to double their power output. Under high light intensity, FDSSCs combined with a condenser also still has a relatively high output power and fill factor, with little performance decline. O'Connor et al. [14] have proposed a new type of solar cell that combines a series of fiber cell units with narrow-band spectrum absorption. A proper arrangement in space is adopted to realize full-spectrum absorption of the sun spectra, resulting in 17% theoretical power convention efficiency. All these above results are difficult to achieve when using planar DSSCs.

FDSSCs act as units, and they are easily encapsulated because only one end or both ends of the capillary need to be sealed during the sealing process [20]. This fact enables the possibility of more conveniently renewing the electrolyte, in contrast to planar DSSCs whose electrolytes cannot be refreshed once they are sealed tightly. In the present paper, the effect of electrolyte refreshing on the photovoltaic performance of FDSSCs was studied. The electron transport and interfacial recombination kinetics were also systematically investigated using electron impedance spectroscopy (EIS).

2. Experimental

2.1. Materials. All chemicals and solvents used were of pure quality. The Ti filament (99.7% pure, diameter = 0.25 mm) was purchased from Alfa Aesar. LiI, I_2, and 4-tetrabutylpyridine (TBP) were purchased from Aldrich. Acetonitrile (CH_3CN, GR: guaranteed reagent) was purchased from Siyou Inc., Tianjin, China. N719 dye ($[(C_4H_9)_4N]_2[Ru(II)L_2(NCS)_2]$, where L = 2,2-bipyridyl-4,4 dicarboxylic acid; ruthenium TBA535) and 1-butyl-3-methylimidazolium iodide (BMII) were from the Dalian Rainbow Light Solar Technology Development Co., Ltd. The TiO_2 colloid was prepared as follows. About 12.0 mL of tetra-butyl titanate (Aldrich) and 2.0 mL of acetic acid were mixed with vigorous stirring. The mixture was slowly dropped into 60.0 mL of water, and 0.5 mL of 65% nitric acid was added to the system. After stirring for 2 h in an oil bath at 80°C, 35 mL of the mixture was transferred into the autoclave and left undisturbed at 220°C for 12 h. After removing part of the solvent, 0.6 g of polyethylene oxide (M_w = 4000; Aldrich) was added and the TiO_2 colloid was ready.

2.2. Fabrication of FDSSCs. The Ti wires were cleaned using acetone, isopropanol, and then ethanol. The Ti wires were immersed into the prepared TiO_2 colloid and dipped in and out several times. Sintering at 400°C for 5 min followed. A thin layer of TiO_2 film was formed on the Ti wire. The above step was repeated until the required thickness of the TiO_2 film was obtained. The TiO_2-coated electrode was sintered at 450°C for 30 min. The electrode was sensitized in a 10^{-4} M N719 ethanol solution for 24 h to obtain the sensitized working electrode. The counterelectrode was a Pt wire 40 μm in diameter. The Pt wire was uniformly and spirally wound onto the photoanode and then inserted into the sealing capillary (0.5 mm inner diameter and 0.85 mm outer diameter) filled with the electrolyte. This electrolyte contained 0.04 M iodine, 0.6 M BMII, 0.05 M LiI, and 0.30 M TBP in acetonitrile. The capillary was sealed with wax to prevent the electrolyte leakage. Each time refreshing the electrolyte, the wax was melted to decapsulate the FDSSC. The used electrolyte was removed, and the unsealed FDSSCs were allowed to suck the fresh electrolyte by capillarity. Finally, the cells were sealed again using wax.

2.3. Measurement and Methods. All device tests and short circuit current responses were conducted on a Keithley Model 2000, with sunlight simulator (YS-55, Japan). The illumination intensity is 100 mW/cm^2. The aperture area of the cell was obtained from the project area A_{pron}, which was equal to twice the sum of the Ti wire diameter and TiO_2 film thickness, multiplied by the length of the device. The short circuit current density J_{sc} was I/A_{proj} (I is the short circuit current). The power conversion efficiency PCE was $J_{\text{sc}} \times V_{\text{oc}} \times \text{FF}/P_{\text{in}}$, where V_{oc} is the open-circuit voltage, FF is the fill factor, and P_{in} is the intensity of incident light. The electrochemical impedance spectrum was obtained using PGSTAT302N (Autolab Corp., Switzerland) within the frequency range of 0.05 Hz to 300 kHz at room temperature and was fitted using Nova 1.7 software.

3. Results and Discussion

Generally, the electrolytes of FTO-glass-based planar DSSCs could not be or difficultly refreshed once there is already an electrolyte leakage. FDSSCs overcome this problem because of their simple and detachable sealing methods [20]. The new issue is whether the electrolyte refreshing times affect the performance of FDSSCs. Figure 1 is an optical photo of FDSSC, in which the details of FDSSC are demonstrated. The FDSSC consists a counterelectrode wrapped around the working electrode, which then encapsulated in a capillary filled with electrolytes. Figure 2 shows the photocurrent density-voltage (J-V) characteristics of devices with electrolyte refreshing

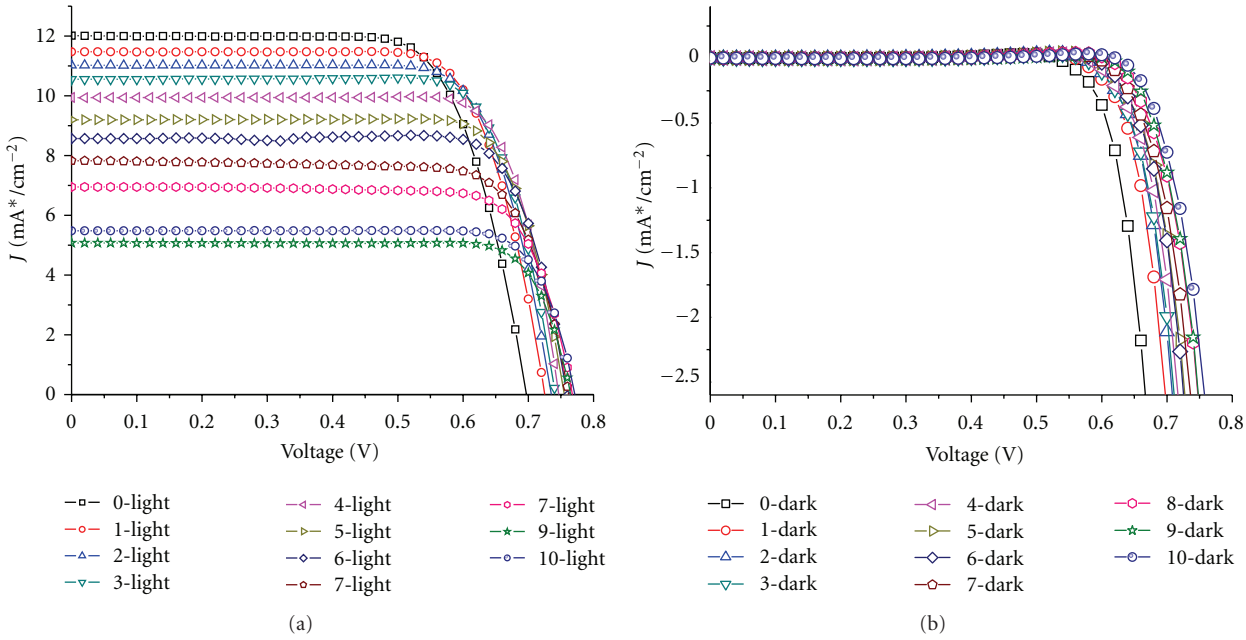

FIGURE 2: (a) Photocurrent density-voltage (J-V) characteristics of devices with electrolyte refreshing times under AM 1.5 illumination (100 mW/cm). (b) J-V curves of the device with electrolyte refreshing times under dark condition.

times under air mass (AM) 1.5 illumination (100 mW/cm^2) (Figure 2(a)) and under dark conditions (Figure 2(b)). The dependency of the photovoltaic performance parameters (J_{sc}, V_{oc}, FF, and PCE) on the electrolyte refreshing times is shown in Figure 3. With increased electrolyte refreshing times from 0 to 10, V_{oc} gradually increased from 0.697 to 0.760 V. FF also increased from 0.730 to 0.820, whereas J_{sc} decreased from 12.01 to 5.07 mA/cm^2. The PCE was at the apex when the electrolyte was refreshed for the first time. At this point, V_{oc}, J_{sc}, FF, and PCE of the FDSSCs were 0.725 V, 11.47 mA/cm^2, 0.749, and 6.23%, respectively. During the second electrolyte refreshing, the PCE began to drop. All these results indicated that certain phenomena occurred inside the FDSSCs when the electrolytes were frequently refreshed.

In a renewable electrochemical system [25, 26]

$$V_{oc} = \left(\frac{kT}{e}\right) \ln\left(\frac{I_{inj}}{n_{cb} k_{et} [I_3^-]}\right), \quad (1)$$

where I_{inj} is the photocurrent injected to the TiO_2 from the excited dye, n_{cb} is the photoelectron density of the conductive band, and k_{et} is the constant of the reaction, and

$$I_3^- + 2e_{cb}(TiO_2) \longrightarrow 3I^-, \quad (2)$$

where I_3^- can enter into tiny cavities inaccessible to dye molecules. The second equation is related to the dark reaction. As shown in Figure 1(b), the dark current density decreased with increased electrolyte refreshing times, especially during the initial stage. This finding meant that, with electrolyte refreshing, the dark reaction was restrained and k_{et} decreased. Consequently, there was less electron recombination between the electrons at the TiO_2 conduction band and I_3^- in the electrolyte. According to (1), V_{oc} increases for the same solar cell if weakened by the dark reaction.

As presented in Figure 3, J_{sc} and PCE also both decreased with increased electrolyte refreshing times. EIS was used to investigate these tendencies. EIS measured in the dark is a well-known technique for studying charge-transfer processes [27–30]. Wide ranges of electrochemical processes and internal resistances that govern the performance of DSSCs could be analyzed by this method. Important general conclusions have been made based on EIS studies. The impedance spectra of DSSCs consist of three components [29, 30], namely, charge transfers at the Pt/electrolyte and TiO_2/electrolyte interfaces, as well as the diffusion of I_3^- in the electrolyte. Each time the electrolyte is refreshed, the impedance data of the FDSSs were acquired at a forward bias of 0.75 V in the dark. Figure 4 shows the Nyquist plots of the corresponding FDSSCs with various electrolyte refreshing times in the dark at an applied forward bias of 0.75 V. The inset in Figure 3 is the equivalent circuit used to fit the experimental data [30, 31]. From left to right in Figure 3, the first arc is the interface between the counterelectrode and electrolyte; the second arc is the interface between TiO_2 and the electrolyte. In the equivalent circuit, R_s is the ohmic serial resistance. R_s represented the transmission resistance of the conducting substrate as well as the interface resistance between the conducting substrate and TiO_2. $R_{ct,CE}$: is the charge transfer resistance, by which the regeneration of I^- at the counterelectrode is characterized. Parallel to $R_{ct,CE}$, the constant phased element (CPE) describes the double-layer capacitance C_{Pt} at the counterelectrode/electrolyte interface.

$$\text{CPE} = Y_0(j\omega)^{-n}, \quad 0 < n \le 1, \; n = 1,$$
$$\text{CPE} = \frac{1}{(j\omega C)}, \quad (3)$$

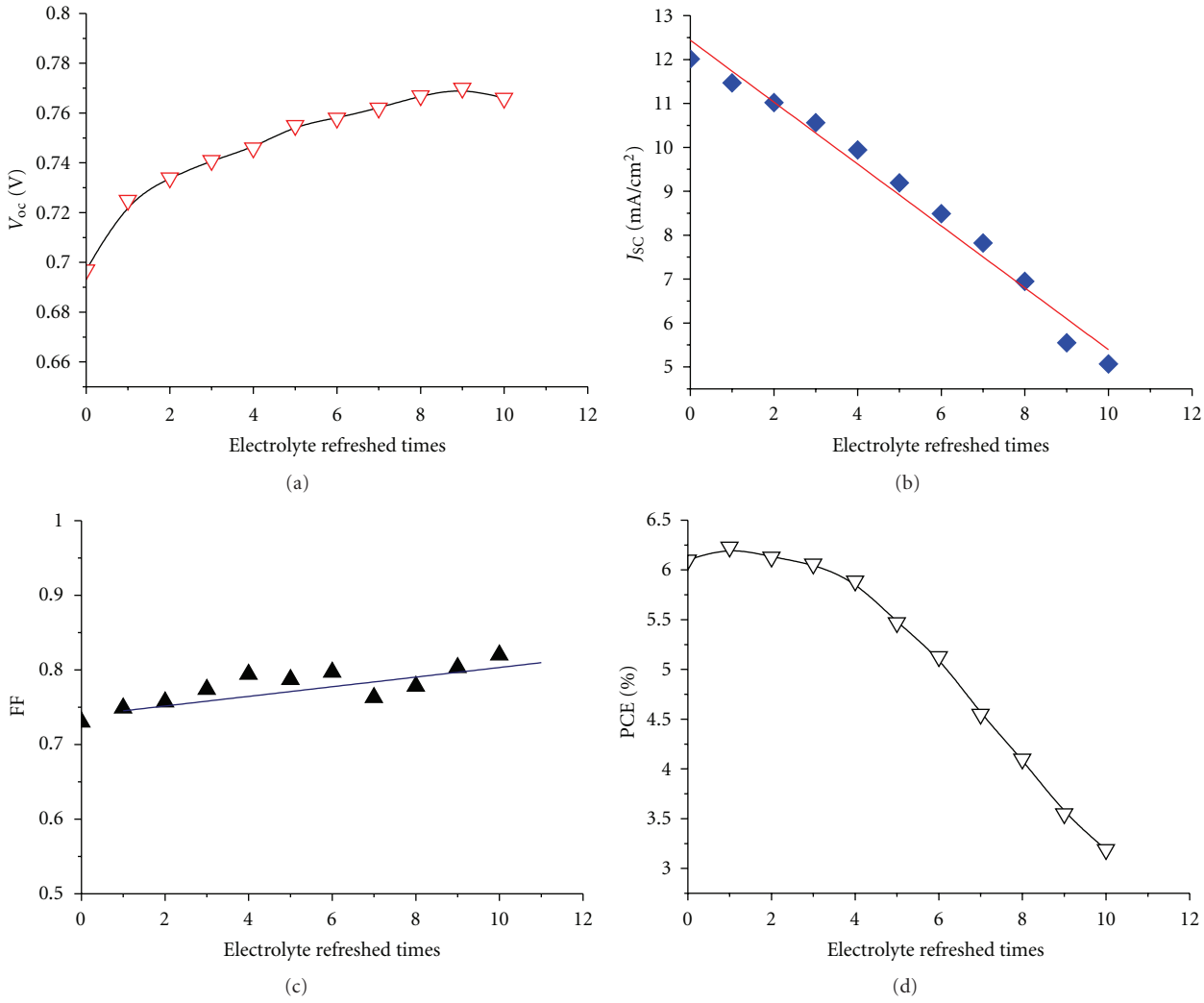

Figure 3: Dependency of V_{oc} (a), J_{sc} (b), FF (c), and PCE (d) on electrolyte refreshing times.

where C is the interface capacitance. $R_{ct,WE}$ and its parallel CPE describe the interfacial charge recombination reaction of electrons with the I_3^- ions and chemical capacitance at TiO_2/electrolyte interface, respectively. W is the impedance for the ion diffusion of electrolytes. For $R_{ct,WE}$ [32, 33],

$$R_{CT,\,WE} = \frac{1}{e}\left(\frac{\partial j_{rec}}{\partial F_n}\right)^{-1} = R_0 \exp\left[-\frac{\beta}{k_B T}(E_{F_n} - E_{redox})\right] = \frac{k_B T \tau}{n_{cb} e^2}, \quad (4)$$

$$\tau = \sqrt{R_{CT,WE} C_\mu}, \quad (5)$$

$$C_\mu = e^2 \frac{\partial n_{cb}}{\partial E_{F_n}} = e^2 \frac{\overline{n}_{cb}}{k_B T}, \quad (6)$$

where j_{rec} is the recombination (or loss) current, E_{Fn} is the position of the Fermi level of electrons, E_{redox} is the potential of the redox couple, $E_{Fn} - E_{redox} = eV_{bias}$, V_{bias} is the potential at the electrode, β is the transfer coefficient, R_0 is a constant, k_B is the Boltzmann constant, T is the absolute temperature, n_{cb} is the electron density of the TiO_2 conduction band, C_μ is the TiO_2/electrolyte interface capacitance, τ is the electron life time, e is the unit charge, F_n is the Fermi level of TiO_2, and $\overline{n}_{cb}$ is the average electron density of the TiO_2 conduction band.

By fitting the experimental data, the useful parameters for understanding the underlying mechanisms of electron transport and recombination were attained, as indicated in Figure 5. The electron combination $R_{ct,WE}$ (Figure 5(a)) increased from 47.8 Ω at the initial to 340 Ω at the tenth electrolyte refreshing. According to (4), at the very same $V_{bias}(E_{Fn} - E_{redox} = eV_{bias})$, the recombination (or loss) current j_{rec} decreases with increased electrolyte refreshing time and electron time τ, as shown in Figure 5(b). Consequently, (7) could be derived as follows [32, 33]:

$$\frac{1}{e}\left(\frac{\partial j_{rec}}{\partial F_n}\right)^{-1} = R_0 \exp\left[-\frac{e\beta}{k_B T} V_{oc}\right]. \quad (7)$$

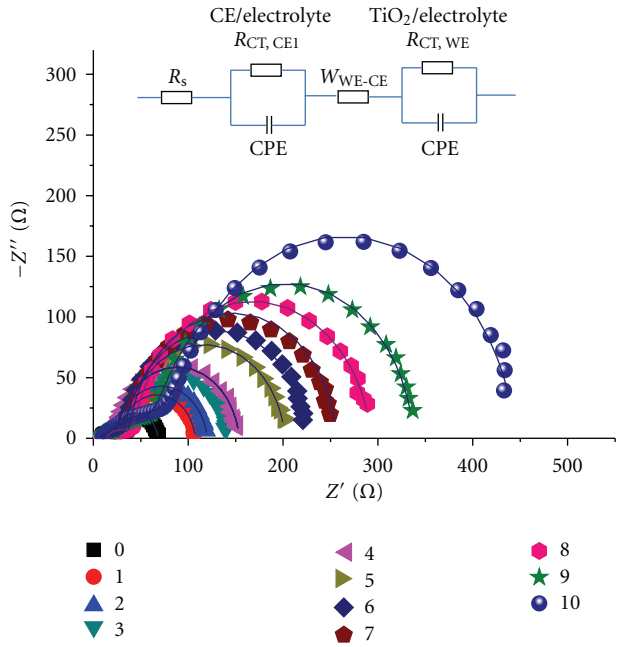

Figure 4: The Nyquist plots of the corresponding DSSCs under various electrolyte refreshing times in the dark at an applied forward bias of −0.75 V. The dot is the experiment data and the line is the fitting data via the inset equivalent circuit.

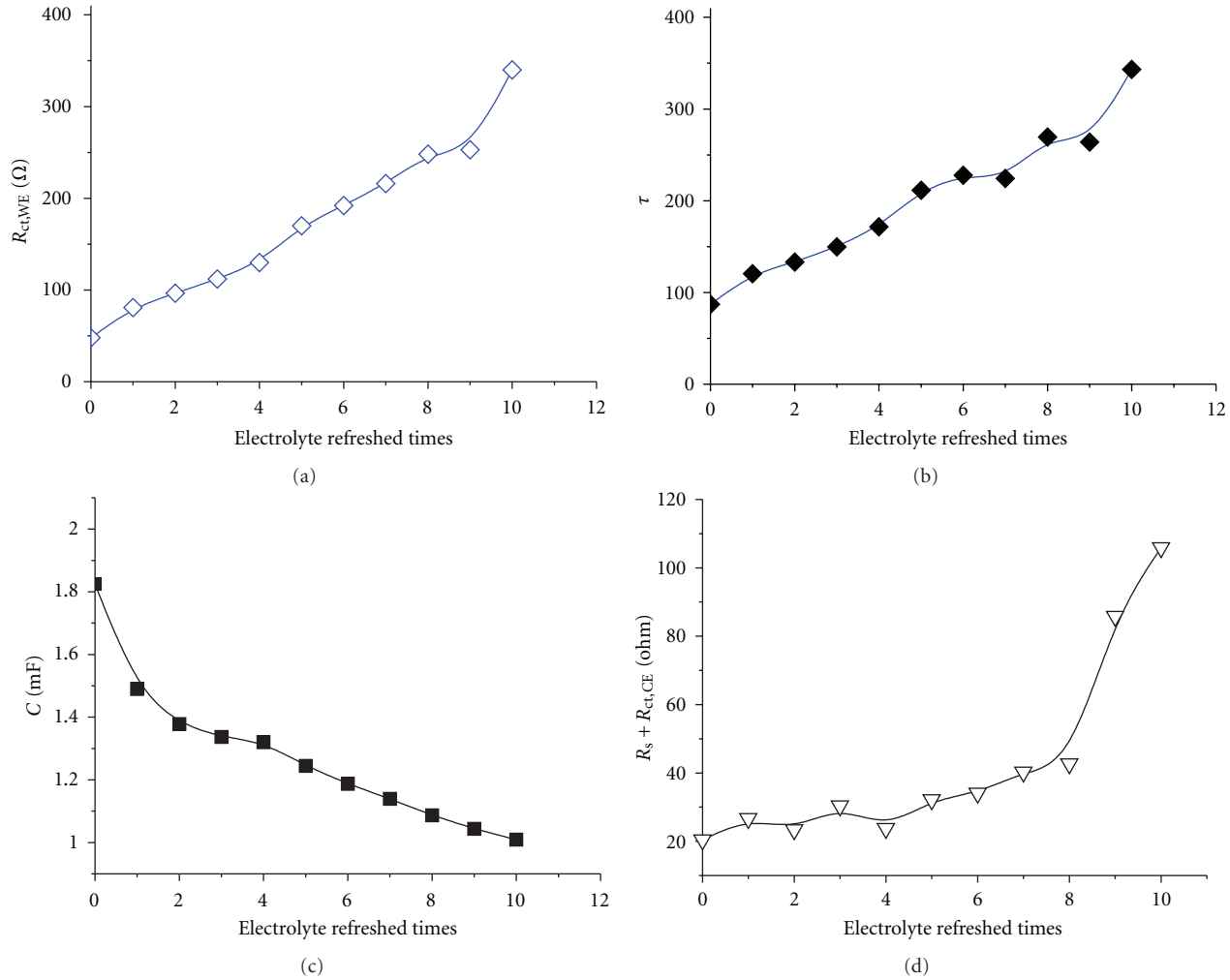

Figure 5: Characteristic parameters $R_{ct,WE}$ (a), electron life time τ (b), chemical capacity C (c), and $R_s + R_{ct,CE}$ (d) of the arc impedance spectra of DSSCs with various electrolyte refreshing times in the dark at an applied forward bias of −0.75 V.

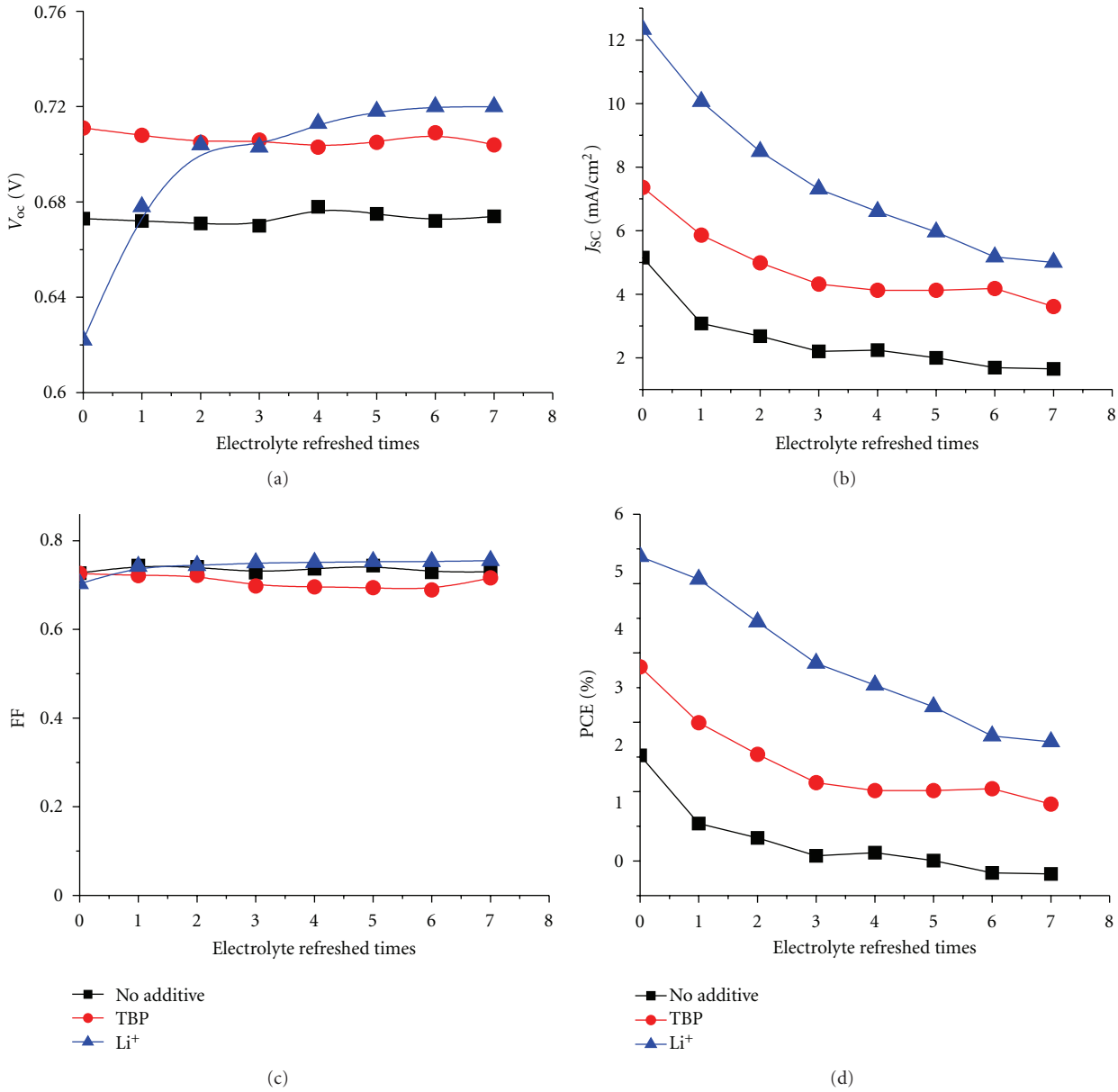

FIGURE 6: *I-V* parameters (V_{oc} (a), J_{sc} (b), FF (c), and PCE (d)) of devices based on different electrolytes varied with electrolyte refreshing times. No additive: 0.04 M I_2 and 0.6 M BMII; TBP: 0.04 M I_2, 0.6 M BMII, and 0.03 M TBP; Li^+: 0.04 M I_2, 0.6 M BMII, and 0.05 M LiI.

Therefore, under the same illumination, there would be less electron recombination and larger V_{oc}. This conclusion was consistent with the dark current shown in Figure 1(b) and with the conclusions derived from (1) and (2).

As aforementioned, J_{sc} declined with electrolyte refreshing. This finding may be ascribed to several aspects. On one hand, it was due to dye desorption. Figure 5(c) shows that the TiO_2/electrolyte interface capacitance C_μ decreased with electrolyte refreshing. According to (6), $\overline{n}_{cb}$ decreases with electrolyte refreshing. This tendency indicates less photocurrent injected into the TiO_2 from the excited dye, which may be due to dye desorption. On the other hand, the increased $R_s + R_{ct,CE}$ with electrolyte refreshing (Figure 5(d)) decreased the J_{sc} [31], which was likely to the electrolyte corrosion of the counter electrolyte [34].

The additive TBP and Li^+ play important roles in maintaining a high V_{oc} [35, 36]. The tendency shown in Figure 3 may be attributed to the remaining additive in the solar cell with electrolyte refreshing. To prove this assumption, the electrolyte refreshing effects on devices based on different electrolytes A, B, and C were investigated. The contents of electrolytes A, B, and C were detailed as follows: A: 0.04 M I_2 and 0.6 M BMII; B: 0.04 M I_2, 0.6 M BMII, and 0.03 M TBP; C: 0.04 M I_2, 0.6 M BMII, and 0.05 M LiI. All the *I-V* parameters of the devices based on A, B, and C are shown in Figure 6. In Figure 5(a), V_{oc} of the devices based on A and B changed little, whereas that of the devices based on C obviously increased with electrolyte refreshing. FF of all the devices only slightly changed with electrolyte refreshing. J_{sc} and PCE of all the devices decline in a similar tendency,

which can be ascribed to the interface charge transport and recombination analyzed in the previous parts. Therefore, we could conclude from Figure 6 that the remaining Li^+ significantly influenced V_{oc} with electrolyte refreshing, the remaining TBP little influenced V_{oc} with electrolyte refreshing and the factors that decreased J_{sc} were mainly related to the decreased PCE. Comparing Figures 3 and 6, we could find that V_{oc} of devices based on electrolyte with both TBP and Li^+ was larger than that of A, B, C, which were based on electrolyte with no additive, with TBP only and with Li^+ only, respectively. It is confirmed that TBP and Li^+ were in synergism to increase V_{oc}.

4. Conclusions

The effect of electrolyte refreshing on the photovoltaic performance of FDSSCs was studied. The electron transport and interfacial recombination kinetics were also systematically investigated by EIS. With increased electrolyte refreshing times from 0 to 10 times, FF and especially V_{oc} increased, whereas J_{sc} and PCE significantly decreased. The increase in V_{oc} was mainly ascribed to less electron recombination with the I_3^- ions as the electrolytes were refreshed according to EIS. Li^+ also played a critical role in V_{oc}, increase and it worked with TBP synergistically to improve V_{oc}. The decline in J_{sc} and PCE was primarily brought about by dye desorption and the increase of series resistance.

Acknowledgments

This work was jointly supported by the NSFC (50833001), MOST (2011CB933300), and MOE (309001) of China.

References

[1] B. O'Regan and M. Grätzel, "A low-cost, high-efficiency solar cell based on dye-sensitized colloidal TiO_2 films," *Nature*, vol. 353, no. 6346, pp. 737–740, 1991.

[2] M. Grätzel, "Photoelectrochemical cells," *Nature*, vol. 414, no. 6861, pp. 338–344, 2001.

[3] M. K. Nazeeruddin, A. Kay, I. Rodicio et al., "Conversion of light to electricity by cis-X2bis(2, 2′-bipyridyl-4, 4′-dicarboxylate)ruthenium(II) charge-transfer sensitizers (X = Cl-, Br-, I-, CN-, and SCN-) on nanocrystalline TiO_2 electrodes," *Journal of the American Chemical Society*, vol. 115, no. 14, pp. 6382–6390, 1993.

[4] J. E. Moser, P. Bonnôte, and M. Grätzel, "Molecular photovoltaics," *Coordination Chemistry Reviews*, vol. 171, no. 1, pp. 245–250, 1998.

[5] L. M. Goncalves, V. De Zea Bermudez, H. A. Ribeiro, and A. M. Mendes, "Dye-sensitized solar cells: a safe bet for the future," *Energy and Environmental Science*, vol. 1, no. 6, pp. 655–667, 2008.

[6] Q. Yu, Y. Wang, Z. Yi et al., "High-efficiency dye-sensitized solar cells: the influence of lithium ions on exciton dissociation, charge recombination, and surface states," *ACS Nano*, vol. 4, no. 10, pp. 6032–6038, 2010.

[7] L. Han, A. Fukui, Y. Chiba et al., "Integrated dye-sensitized solar cell module with conversion efficiency of 8.2%," *Applied Physics Letters*, vol. 94, no. 1, Article ID 013305, 2009.

[8] X. Fan, Z. Chu, F. Wang, L. Chen, Y. Tang, and D. Zou, "Wire-shaped flexible dye-sensitized solar cells," *Advanced Materials*, vol. 20, no. 3, pp. 592–595, 2008.

[9] M. R. Lee, R. D. Eckert, K. Forberich, G. Dennler, C. J. Brabec, and R. A. Gaudiana, "Solar power wires based on organic photovoltaic materials," *Science*, vol. 324, no. 5924, pp. 232–235, 2009.

[10] H. Wang, Y. Liu, M. Li, H. Huang, M. Zhong, and H. Shen, "Hydrothermal growth of large-scale macroporous TiO_2 nanowires and its application in 3D dye-sensitized solar cells," *Applied Physics A*, vol. 97, no. 1, pp. 25–29, 2009.

[11] B. Weintraub, Y. G. Wei, and Z. L. Wang, "Optical fiber/nanowire hybrid structures for efficient three-dimensional dye-sensitized solar cells," *Angewandte Chemie*, vol. 48, no. 47, pp. 8981–8985, 2009.

[12] S. Huang, Q. Zhang, X. Huang et al., "Fibrous CdS/CdSe quantum dot co-sensitized solar cells based on ordered TiO_2 nanotube arrays ," *Nanotechnology*, vol. 21, no. 37, Article ID 375201, 2010.

[13] Y. Liu, M. Li, H. Wang et al., "Synthesis of TiO_2 nanotube arrays and its application in mini-3D dye-sensitized solar cells," *Journal of Physics D*, vol. 43, no. 20, 2010.

[14] B. O'Connor, D. Nothern, K. P. Pipe, and M. Shtein, "High efficiency, broadband solar cell architectures based on arrays of volumetrically distributed narrowband photovoltaic fibers," *Optics Express*, vol. 18, no. 19, pp. A432–A443, 2010.

[15] D. Zou, D. Wang, Z. Chu, Z. Lv, and X. Fan, "Fiber-shaped flexible solar cells," *Coordination Chemistry Reviews*, vol. 254, no. 9-10, pp. 1169–1178, 2010.

[16] J. Bae, Y. J. Park, M. Lee et al., "Single-fiber-based hybridization of energy converters and storage units using graphene as electrodes," *Advanced Materials*, vol. 23, no. 30, pp. 3446–3449, 2011.

[17] T. Chen, S. Wang, Z. Yang et al., "Flexible, light-weight, ultrastrong, and semiconductive carbon nanotube fibers for a highly efficient solar cell," *Angewandte Chemie*, vol. 50, no. 8, pp. 1815–1819, 2011.

[18] Y. Fu, Z. Lv, S. Hou et al., "Conjunction of fiber solar cells with groovy micro-reflectors as highly efficient energy harvesters," *Energy and Environmental Science*, vol. 4, no. 9, pp. 3379–3383, 2011.

[19] S. Huang, X. Guo, X. Huang et al., "Highly efficient fibrous dye-sensitized solar cells based on TiO_2 nanotube arrays," *Nanotechnology*, vol. 22, no. 31, Article ID 315402, 2011.

[20] Z. Lv, Y. Fu, S. Hou et al., "Large size, high efficiency fiber-shaped dye-sensitized solar cells," *Physical Chemistry Chemical Physics*, vol. 13, no. 21, pp. 10076–10083, 2011.

[21] D. Wang, S. Hou, H. Wu, C. Zhang, Z. Chu, and D. Zou, "Fiber-shaped all-solid state dye sensitized solar cell with remarkably enhanced performance via substrate surface engineering and TiO_2 film modification," *Journal of Materials Chemistry*, vol. 21, no. 17, pp. 6383–6388, 2011.

[22] J. Yu, D. Wang, Y. Huang et al., "A cylindrical core-shell-like TiO_2 nanotube array anode for flexible fiber-type dye-sensitized solar cells," *Nanoscale Research Letters*, vol. 6, article 94, 2011.

[23] K. Okada, H. Matsui, T. Kawashima, T. Ezure, and N. Tanabe, "100 mm × 100 mm large-sized dye sensitized solar cells," *Journal of Photochemistry and Photobiology A*, vol. 164, no. 1–3, pp. 193–198, 2004.

[24] M. A. Green, "Consolidation of thin-film photovoltaic technology: the coming decade of opportunity," *Progress in Photovoltaics*, vol. 14, no. 5, pp. 383–392, 2006.

[25] M. L. Rosenbluth and N. S. Lewis, "'Ideal' behavior of the open circuit voltage of semiconductor/liquid junctions," *The Journal of Physical Chemistry*, vol. 93, no. 9, pp. 3735–3740, 1989.

[26] A. Kumar, P. G. Santangelo, and N. S. Lewis, "Electrolysis of water at SrTiO3 photoelectrodes: distinguishing between the statistical and stochastic formalisms for electron-transfer processes in fuel-forming photoelectrochemical systems," *The Journal of Physical Chemistry*, vol. 96, no. 2, pp. 834–842, 1992.

[27] J. Bisquert, "Theory of the impedance of electron diffusion and recombination in a thin layer," *The Journal of Physical Chemistry B*, vol. 106, no. 2, pp. 325–333, 2002.

[28] J. Bisquert, A. Zaban, and P. Salvador, "Analysis of the mechanisms of electron recombination in nanoporous TiO_2 dye-sensitized solar cells. Nonequilibrium steady-state statistics and interfacial electron transfer via surface states," *The Journal of Physical Chemistry B*, vol. 106, no. 34, pp. 8774–8782, 2002.

[29] I. Morá-Seró and J. Bisquert, "Effect of reduced selectivity of contacts on the current-potential characteristics and conversion performance of solar cells," *Solar Energy Materials and Solar Cells*, vol. 85, no. 1, pp. 51–62, 2005.

[30] Q. Wang, J. E. Moser, and M. Grätzel, "Electrochemical impedance spectroscopic analysis of dye-sensitized solar cells," *The Journal of Physical Chemistry B*, vol. 109, no. 31, pp. 14945–14953, 2005.

[31] Q. Wang, S. Ito, M. Grätzel et al., "Characteristics of high efficiency dye-sensitized solar cells," *The Journal of Physical Chemistry B*, vol. 110, no. 50, pp. 25210–25221, 2006.

[32] F. Fabregat-Santiago, J. Bisquert, E. Palomares et al., "Correlation between photovoltaic performance and impedance spectroscopy of dye-sensitized solar cells based on ionic liquids," *The Journal of Physical Chemistry C*, vol. 111, no. 17, pp. 6550–6560, 2007.

[33] I. Mora-Seró, J. Bisquert, F. Fabregat-Santiago et al., "Implications of the negative capacitance observed at forward bias in nanocomposite and polycrystalline solar cells," *Nano Letters*, vol. 6, no. 4, pp. 640–650, 2006.

[34] T. N. Murakami, S. Ito, Q. Wang et al., "Highly efficient dye-sensitized solar cells based on carbon black counter electrodes," *Journal of the Electrochemical Society*, vol. 153, no. 12, Article ID 047612JES, pp. A2255–A2261, 2006.

[35] S. Rühle, M. Greenshtein, S. G. Chen et al., "Molecular adjustment of the electronic properties of nanoporous electrodes in dye-sensitized solar cells," *The Journal of Physical Chemistry B*, vol. 109, no. 40, pp. 18907–18913, 2005.

[36] K. Ryuzi, K. Motohiro, S. Kodate, A. Furube, N. Fuke, and N. Koide, "Effects of 4-tert-butylpyridine and li ions on photoinduced electron injection efficiency in black-dye-sensitized Nanocrystalline TiO_2 films," *The Journal of Physical Chemistry C*, vol. 113, no. 48, pp. 20738–20744, 2009.